



저작자표시-비영리-변경금지 2.0 대한민국

이용자는 아래의 조건을 따르는 경우에 한하여 자유롭게

- 이 저작물을 복제, 배포, 전송, 전시, 공연 및 방송할 수 있습니다.

다음과 같은 조건을 따라야 합니다:



저작자표시. 귀하는 원저작자를 표시하여야 합니다.



비영리. 귀하는 이 저작물을 영리 목적으로 이용할 수 없습니다.



변경금지. 귀하는 이 저작물을 개작, 변형 또는 가공할 수 없습니다.

- 귀하는, 이 저작물의 재이용이나 배포의 경우, 이 저작물에 적용된 이용허락조건을 명확하게 나타내어야 합니다.
- 저작권자로부터 별도의 허가를 받으면 이러한 조건들은 적용되지 않습니다.

저작권법에 따른 이용자의 권리는 위의 내용에 의하여 영향을 받지 않습니다.

이것은 [이용허락규약\(Legal Code\)](#)을 이해하기 쉽게 요약한 것입니다.

[Disclaimer](#)

Protective role of bilirubin nanoparticle on heart  
ischemia-reperfusion injury

Juhan Lee

The Graduate School  
Yonsei University  
Department of Medicine

# Protective role of bilirubin nanoparticle on heart ischemia-reperfusion injury

A Dissertation Submitted  
to the Department of Medicine  
and the Graduate School of Yonsei University  
in partial fulfillment of the  
requirements for the degree of  
Doctor of Philosophy in Medical Science

Juhan Lee

June 2024

**This certifies that the Dissertation  
of Juhan Lee is approved.**



Thesis Supervisor [Kyu Ha Huh]



Thesis Committee Member [Beom Seok Kim]



Thesis Committee Member [Dong Jin Joo]



Thesis Committee Member [Hyung Joon Ahn]



Thesis Committee Member [Beom Jin Lim]

**The Graduate School  
Yonsei University  
June 2024**

## ACKNOWLEDGEMENTS

I extend my deepest and sincerest gratitude to my supervisor, Dr. Kyu Ha Huh, for his invaluable guidance and unwavering support throughout the course of this research. Additionally, I am profoundly thankful to my former supervisor, Dr. Yu Seun Kim, whose mentorship and encouragement have left a lasting impact on my academic journey.

I wish to express profound gratitude to Dr. Dong Jin Joo for providing invaluable research insights and networking opportunities.

I would also like to thank my thesis committee: Dr. Beom Seok Kim, Dr. Hyung Joon Ahn, and Dr. Beom Jin Lim, for their insightful feedback and valuable suggestions, which have greatly contributed to the improvement of this work.

I extend a special note of gratitude to Dr. Myoung Soo Kim and The Research Institute for Transplantation for providing the necessary resources and facilities. I am particularly grateful to Dr. Soo Jin Kim and Yuri Cho for their dedicated assistance throughout this project.

To my family, I extend heartfelt appreciation for their unwavering love, support, and belief in my abilities. I am indebted to my father for

instilling in me a passion for scholarship, and to my mother for her enduring love. Sophia and Emily, my beloved daughters, your presence has been my greatest inspiration to strive for excellence. Darae, my wife and best friend, thank you for your unwavering love and support.

This work would not have been possible without the collective effort and contributions of all those mentioned above. Thank you.

Juhan Lee

## TABLE OF CONTENTS

LIST OF FIGURES .....	iii
LIST OF TABLES .....	iv
ABSTRACT IN ENGLISH .....	v
1. INTRODUCTION .....	1
2. MATERIALS AND METHODS .....	2
2.1. Animal and reagents .....	2
2.1.1. Animals .....	2
2.1.2. Bilirubin nanoparticle .....	2
2.1.3. Experimental procedures .....	3
2.1.3.1. Sham group .....	4
2.1.3.1. Ischemia-reperfusion injury group .....	5
2.1.3.1. Ischemia-reperfusion injury + bilirubin nanoparticle treatment group .....	5
2.2. Histology .....	5
2.2.1. Triphenyltetrazolium chloride staining .....	5
2.2.2. Terminal deoxynucleotidyl transferase dUTP nick end labeling staining .....	5
2.3. Proteomics analysis .....	6
2.3.1. Tissue Preservation for Analysis .....	6
2.3.2. Protein extraction .....	6
2.3.3. Trypsin digestion with S-Trap .....	6
2.3.4. Tandem mass tag-labeling and reverse phase-high performance liquid chromatography fractionation .....	7
2.3.5. Nano liquid chromatography tandem mass spectrometry .....	8
2.3.6. Integrated proteomics pipeline search and bioinformatic analysis .....	10
3. RESULTS .....	11
3.1. Histological assessments of ischemia reperfusion injury .....	11
3.2.1. Effect of BX-001N treatment on myocardial tissue damage in rat IRI models .....	11
3.2.2. Effect of BX-001N treatment on myocardial apoptosis in rat IRI models .....	11
3.2. LC-MS/MS proteomics profiling .....	14
3.3. Bioinformatic analysis .....	18
4. DISCUSSION .....	30
5. CONCLUSION .....	35
REFERENCES .....	36

ABSTRACT IN KOREAN ..... 41

## LIST OF FIGURES

<Fig 1> Structures of bilirubin nanoparticles .....	3
<Fig 2> Myocardial ischemia-reperfusion injury model in rat .....	4
<Fig 3> Schematic illustration of the experimental steps .....	9
<Fig 4> TTC staining analysis .....	12
<Fig 5> TUNEL staining .....	13
<Fig 6> The Pearson correlation for each sample .....	15
<Fig 7> The heatmap of clustered samples revealed distinct patterns for each cluster .....	17
<Fig 8> The outcomes of pathway analysis enriched via the Metascape web tool .....	24
<Fig 9> Pathway analysis results utilizing STRING database .....	26
<Fig 10> Pathway analysis results utilizing KEGG .....	28

## LIST OF TABLES

<Table 1> Results of pathway analysis using the Metascape tool for cluster 0.....	19
<Table 2> Results of pathway analysis using the Metascape tool for cluster 1.....	22
<Table 3> Effect of Wnt signaling pathways during myocardial ischemia-reperfusion injury .....	32
<Table 4> Therapeutic strategies targeting Wnt signaling for the treatment of ischemia-reperfusion injury .....	33

## ABSTRACT

### **Protective role of bilirubin nanoparticle on heart ischemia-reperfusion injury**

In the context of myocardial infarction, ischemia-reperfusion injury (IRI) represents a significant therapeutic challenge, with current treatments are insufficient in effectively mitigating the associated tissue damage. IRI occurs paradoxically with the restoration of blood flow following ischemia, exacerbating initial tissue damage through oxidative stress and inflammatory responses. Bilirubin, an endogenous metabolite resulting from heme catabolism, has emerged as a potential therapeutic agent for its antioxidant and anti-inflammatory properties. This study investigated the efficacy of bilirubin nanoparticles in rat models of myocardial IRI, employing proteomic analysis through liquid chromatography-tandem mass spectrometry (LC-MS/MS) to elucidate underlying mechanisms. Treatment with bilirubin nanoparticles significantly attenuated myocardial infarction and apoptosis in a dose-responsive manner. Proteomic profiling identified 3,616 protein groups and 76,681 unique peptides, with clustering analysis delineating proteins based on their expression patterns. Notably, 202 proteins were downregulated in the IRI model and showed recovery after treatment with bilirubin nanoparticles, whereas 35 proteins were upregulated in response to IRI and exhibited recovery following bilirubin treatment. Pathway analysis underscored significant enhancements in the Wnt signaling and insulin signaling pathways, along with increased Golgi apparatus markers, indicating their roles in mediating the protective effects of bilirubin nanoparticles against myocardial IRI. These findings advance the proteomic landscape associated with myocardial IRI and propose

bilirubin nanoparticles as an effective strategy for cardiac protection, warranting further investigation in human clinical settings.

---

Key words : ischemia-reperfusion injury, heart, bilirubin nanoparticle, proteomics

## I. INTRODUCTION

Ischemia is a pathological condition characterized by insufficient blood flow and oxygen supply to tissues or organs.<sup>1</sup> It contributes to various severe diseases, including myocardial infarction, ischemic heart disease, cerebral infarction, and transplant organ damage.<sup>2,3</sup> During ischemia, oxidative phosphorylation via the electron transport chain is reduced, resulting in accumulation of superoxide radicals along with decreased adenosine triphosphate. Ischemic conditions further disrupt ionic, acid-base, and protein homeostasis, exacerbating organ dysfunction.<sup>4</sup> Although timely reperfusion is crucial for reducing ischemic damage, it can paradoxically lead to ischemia-reperfusion injury (IRI), worsening tissue damage.<sup>1,5,6</sup> This occurs through various mechanisms, including oxidative stress, inflammation, and cell death.<sup>2,7</sup> Despite numerous attempts to mitigate IRI, an effective treatment remains elusive.<sup>8</sup>

Bilirubin, a metabolite of heme primarily derived from aged or damaged red blood cells, was historically deemed toxic.<sup>9</sup> Recent studies, however, have revealed that bilirubin possesses potent antioxidant effects in the body.<sup>10,11</sup> Additionally, bilirubin demonstrates the ability to reduce inflammatory responses and inhibit vascular smooth muscle cell proliferation.<sup>12</sup> These attributes offer a promising avenue for mitigating IRI, as evidenced by bilirubin's inverse correlation with cardiovascular disease severity and mortality.<sup>13,14</sup> Furthermore, emerging research underscores its protective effects against IRI in vital organs such as the heart, liver, and kidney.<sup>15-17</sup> Although it is presumed that bilirubin's antioxidant or anti-inflammatory effects contribute to its protective role, the specific mechanisms are not fully understood.

The objective of this study was to evaluate the underlying mechanism of bilirubin nanoparticle treatment against myocardial IRI. We employed a rat model of myocardial IRI treated with bilirubin nanoparticles. A proteomics-driven approach was applied to identify the effects of IRI and the impact of bilirubin nanoparticle treatment.

## 2. MATERIALS AND METHODS

### 2.1. *Animals and reagents*

#### 2.1.1. Animals

Male Sprague–Dawley rats, aged 8–9 weeks and weighing 290–320 g, were purchased from Orient Bio (Orient bio Inc., Seongnam, Republic of Korea). The rats were maintained in a controlled environment with a temperature of  $22 \pm 2$  °C, humidity at  $60 \pm 6\%$ , and a consistent 12:12-hour light-dark cycle. The light phase starting at 8 A.M. and all experimental procedures were conducted during this light phase. This study was conducted in accordance with the institutional guidelines on the use of live animals for research, and the experimental protocol was approved by the Institutional Animal Care and Use Committee of Yonsei University Health System.

#### 2.1.2. Bilirubin nanoparticle

Despite the recognized antioxidant and anti-inflammatory effects of bilirubin, its clinical application has been significantly constrained by inherent challenges related to its insolubility and rapid systemic clearance.<sup>18,19</sup> To overcome these challenges, a novel pharmaceutical approach by conjugating bilirubin with polyethylene glycol (PEG) has been developed. In this study, we used self-assembled mono-PEGylated bilirubin 3 $\alpha$  nanoparticle, consisting of 36 ethylene oxide moieties and one synthetic bilirubin 3 $\alpha$ , covalently bonded (BX-001N, Figure 1).<sup>20,21</sup> BX-001N was provided by Bilix Co., Ltd. (Yongin, Republic of Korea).

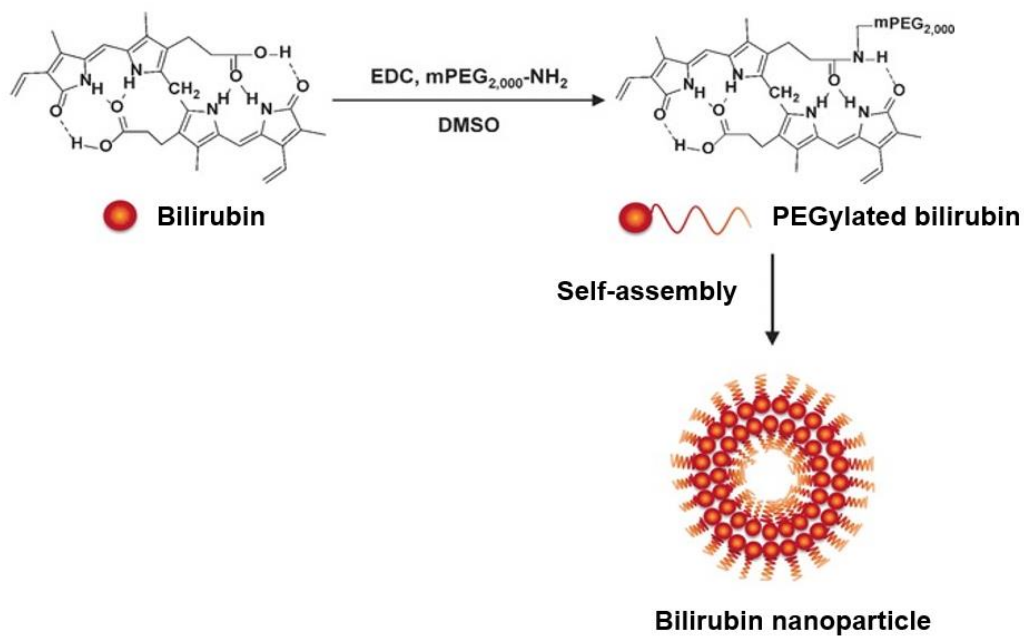


**Figure 1.** Structures of bilirubin nanoparticles.

### 2.1.3. Experimental procedures

All rats were anesthetized using 3% isoflurane, with maintenance via tracheal intubation. Ventilation parameters were controlled at 60–80 breaths per minute, with a tidal volume of 2–3 mL/100 g body weight. During the procedures, the body temperature of each rat was consistently maintained at 36.5–37.5 °C using a heating pad. The chest wall and pericardium were dissected in all rats to reveal the heart. The left anterior descending coronary artery (LAD) was exposed, and a 5-0 silk ligature was placed beneath it, threaded through a small plastic tube to enable reversible LAD occlusion (Figure 2).

### 2.1.3.1. Sham group

Rats underwent the same surgical procedures as the IRI group, including LAD exposure and ligature placement, but without actual LAD occlusion, serving as a control. Normal saline was administered intravenously at the same time points as in the IRI group. For control, BX-001N (40 mg/kg) was administered intravenously.

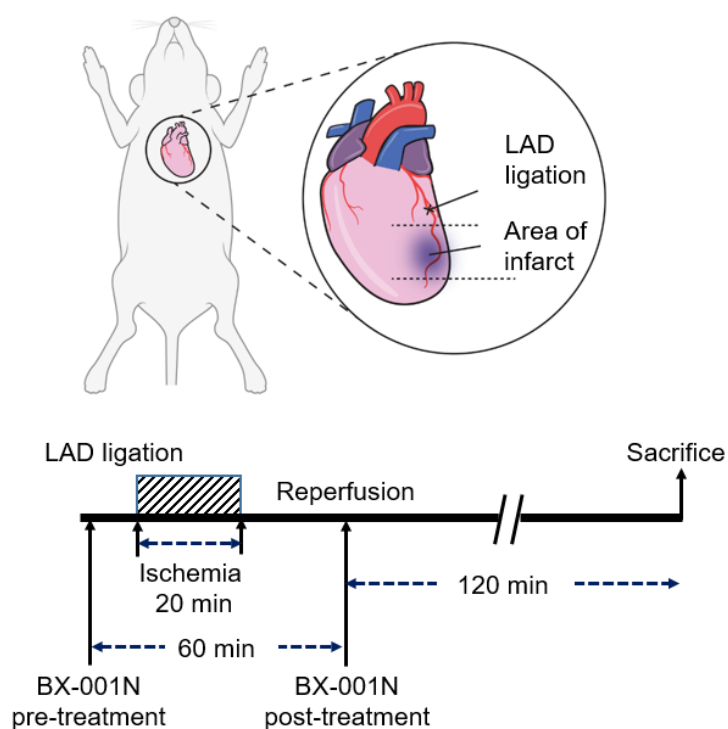


**Figure 2.** Myocardial ischemia-reperfusion injury model in rat. Ischemia was induced by ligating the left anterior descending coronary artery (LAD) for 20 minutes, followed by a reperfusion. The first dose of bilirubin nanoparticle (BX-001N) was administered five minutes before inducing ischemia, and the second dose 35 minutes after reperfusion, with an interval of one hour between the two administrations.

#### 2.1.3.2. Ischemia-reperfusion injury group

Ischemia was induced in this group by ligating the LAD for 20 minutes, followed by a reperfusion period of 120 minutes. A corresponding volume of normal saline was injected intravenously at the same time points as the BX-001N administration.

#### 2.1.3.3. Ischemia-reperfusion injury + bilirubin nanoparticle treatment group

BX-001N was dissolved in 100% normal saline and administered intravenously at 20 mg/kg and 40 mg/kg through the tail vein. The first dose was administered five minutes before inducing ischemia, and the second dose 35 minutes after reperfusion, with an interval of one hour between the two administrations.

## 2.2. *Histology*

### 2.2.1. Triphenyltetrazolium chloride staining

2,3,5-Triphenyltetrazolium chloride (TTC) staining was conducted to evaluate myocardial viability. Myocardial tissue sections were incubated in a TTC solution at 37°C for 20 minutes. Viable myocardial tissues were identified by the development of a red precipitate, indicative of the enzymatic conversion of TTC to formazan within live cells. In stark contrast, necrotic regions did not stain and remained colorless, thereby providing a distinct contrast between viable and non-viable myocardial regions. Subsequent to the staining procedure, the tissue sections were fixed, photographed for documentation, and meticulously analyzed to determine the extent of myocardial infarction.

### 2.2.2. Terminal deoxynucleotidyl transferase dUTP nick end labeling staining

To detect apoptosis in myocardial tissue, we performed Terminal deoxynucleotidyl transferase dUTP nick end labeling (TUNEL) staining on 5- $\mu$ m thick paraffin-embedded sections using the TUNEL assay kit (R&D Systems, MN, USA), following the manufacturer's instructions. The

TUNEL reaction was visualized using HRP-labeled streptavidin and DAB solution, and sections were counterstained with Methyl Green. After dehydration and clearing, slides were mounted with mounting medium. The result was viewed under a light microscope at magnification, x200. The statistical significance between means was determined with a one-way ANOVA. A significance level of  $p$ -value  $< 0.05$  was used with Tukey's method using GraphPad Prism software (Version 8.0.1).

### 2.3. *Proteomics analysis*

#### 2.3.1. Tissue Preservation for Analysis

The intact heart area was dissected and fixed in 10% neutral buffered formalin for 48 hours before embedding in paraffin. Corresponding myocardial tissue was quickly frozen in liquid nitrogen and stored at  $-80$  °C for protein analysis.

#### 2.3.2. Protein extraction

The myocardium tissues were homogenized in the RIPA buffer supplemented with protease and phosphatase inhibitor mixture (Thermo Fisher Scientific, MA, USA). The lysates were then centrifuged. The protein concentration of the supernatants was quantified using the Protein Assay Dye (BIO-RAD Laboratories, CA, USA).

#### 2.3.3. Trypsin digestion with S-Trap method

We have performed sample preparation for LC-MS/MS with following methods of Cho et al. and minor modification.<sup>22</sup> A Protifi S-Trap<sup>TM</sup> mini spin column (C02-mini-80, Protifi, USA) was employed to process each sample following the guidelines provided by the manufacturer. Specifically, 300  $\mu$ g of proteins in SDS 5% buffer, treated with 5 mM TCEP (final concentration) at 55 °C for 15 minutes, underwent reduction. Subsequently, alkylation was performed with 20 mM iodoacetamide (final concentration) at room temperature for 10 minutes in the absence of light. Phosphoric acid was introduced to the alkylated proteins, reaching a final concentration of 1.2%,

and acidified proteins were combined with six volumes of binding buffer (90% methanol; 100 mM TEAB; pH 7.1). The resulting mixture was applied to the S-Trap column, followed by centrifugation at 4,000 g for 30 seconds to capture proteins. Next, 400  $\mu$ L of wash buffer (90% methanol; 100mM TEAB; pH 7.1) was added three times to cleanse the proteins. Finally, the proteins were subjected to digestion with trypsin gold (V5280, Promega, WI, USA) at 37 °C overnight, maintaining a protein-to-enzyme ratio of 10:1 (w/w). The digested peptides were eluted through a three-step process, using 80  $\mu$ L of 50 mM TEAB in water, 0.2% formic acid in water, and 50% acetonitrile in water, respectively, at 4,000 g for 1 minute. The pooled peptide solution was then dried using a speed-vacuum.

#### 2.3.4. Tandem mass tag-labeling and reverse phase-high performance liquid chromatography fractionation

Peptide samples quantified at 100  $\mu$ g using the Quantitative Colorimetric Peptide Assay (cat#23275, Thermo Fisher Scientific, MA, USA) were dissolved in 100  $\mu$ L of 100 mM TEAB. Tandem mass tag (TMT)-10 and 11 reagents (cat#37725, Thermo Fisher Scientific, MA, USA) were re-suspended in acetonitrile to a concentration of 10  $\mu$ g/ $\mu$ L. The TMT reagent was added to each sample, mixed, and incubated for 1 hour at 25 °C at 800 rpm. Subsequently, the reaction was quenched with 5% hydroxylamine and incubated for 15 minutes at 25 °C at 800 rpm. For quality control, half of each plex was combined to create a quality control (QC) sample, allowing for an assessment of the success of TMT labeling on liquid chromatography-tandem mass spectrometry (LC-MS/MS). The dried QC sample was reconstituted in water and subjected to analysis using a NexeraXR HPLC system (LC-20AD, Shimadzu, Japan). The analysis involved a 70-minute gradient, transitioning from 5% to 95% mobile phase B (5 mM ammonium formate in 95% ACN) at a flow rate of 0.5 mL/min. Mobile phase A consisted of 5 mM ammonium formate in distilled water. Subsequently, fractionation was performed using an FRC-10 (FRC-10A, Shimadzu, Japan), collecting samples over 20 minutes at one minute intervals. The resulting 40 fractions were

combined into 20 fractions and dissolved in 0.1% formic acid for subsequent LC-MS/MS analysis.

### 2.3.5. Nano liquid chromatography tandem mass spectrometry

Twenty dissolved samples in 0.1% formic acid were subjected to analysis using an LC-MS/MS system comprising an UltiMate 3000 RS LC-nano system (Thermo Fisher Scientific, MA, USA) and an Orbitrap Eclipse Tribrid mass spectrometer (Thermo Fisher Scientific, MA, USA) equipped with a nano electrospray source. An autosampler facilitated the loading of sample solutions into a C18 trap column (Acclaim PepMap™ 100, 75  $\mu\text{m} \times 2$  cm; 164535, Thermo Fisher Scientific, MA, USA), where samples underwent desalting and concentration for 9.5 minutes at a flow rate of 4  $\mu\text{L}/\text{min}$ . Subsequently, the trapped samples were separated on a C18 analytical column (PepMap™ RSLC C18, 2  $\mu\text{m}$ , 100  $\text{\AA}$ , 75  $\mu\text{m} \times 50$  cm; ES903, Thermo Fisher Scientific, MA, USA). The mobile phases consisted of 99.9% water (A) and 99.9% ACN (B), each containing 0.1% formic acid. The LC gradient initiated with 5% of B for 10 minutes, followed by a ramp to 13% of B for 40 minutes, 25% of B for 65 minutes, and 95% of B for 5 minutes. This was succeeded by a 5-minute hold at 95% of B and 5% of B for an additional 1 minute. The column was re-equilibrated with 5% of B for 14 minutes before the next run. A voltage of 2,100 V was applied for ionization.

Throughout the chromatographic separation, the Orbitrap Eclipse Tribrid mass spectrometer (Thermo Fisher Scientific, MA, USA) operated in a data-dependent mode, automatically transitioning between MS1 and MS2. Full-scan MS1 spectra (400–2,000  $m/z$ ) were acquired by the Orbitrap at a resolution of 120,000, with an automatic maximum ion injection time and an AGC target value of  $4.0 \times 10^5$ . MS2 spectra were obtained by the Orbitrap mass analyzer at a resolution of 30,000, utilizing HCD (36% normalized collision energy, maximum ion injection time of 50 ms, AGC target value of  $5.0 \times 10^4$ ). Previously fragmented ions were excluded for 30 seconds within a 10 ppm range. Sequential experimental steps undertaken in our study are illustrated in Figure 3.

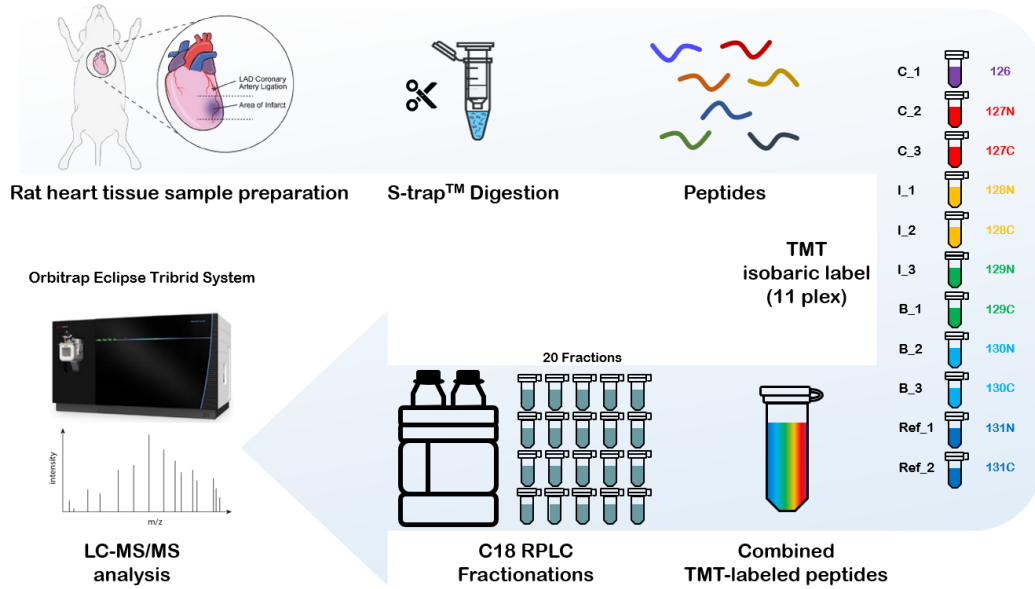


**Figure 3.** Schematic illustration of the experimental steps. A total of 9 rat heart tissue samples [(C, Sham = 3), (I, IRI = 3), (B, IRI + BX-001N 40mg/kg = 3)] were digested into peptides using S-trap method. Each sample was labeled with TMT-11plex, including pooled reference samples. The combined TMT-labeled peptides were fractionated by high basic pH reverse phase-high performance liquid chromatography.

### 2.3.6. Integrated proteomics pipeline search and bioinformatic analysis

The MS/MS spectra were subjected to analysis utilizing the E. Integrated proteomics pipeline (IP2) search algorithm (Integrated Proteomics Applications, Inc., CA, USA) in conjunction with the UniProt human protein database (March 2021, containing reviewed proteins). To assess false discovery rate (FDR), the reverse sequences of all proteins were incorporated into the database. Peptide identification was carried out using ProLuCID, specifying a precursor mass error of 5 ppm and a fragment ion mass error of 50 ppm. The enzyme trypsin was chosen, allowing for two potential missed cleavages. TMT modification (+229.1629) at the N-terminus and lysine residue, along with carbamidomethylation at cysteine, were designated as static modifications. Methionine oxidation was considered a variable modification.

Post-analysis, output data files were filtered and organized using DTASelect (The Scripps Research Institute, CA, USA) with a requirement of two or more peptide assignments per protein for identification, maintaining a false positive rate below 0.01. Quantitative analysis was conducted using Census within the IP2 pipeline. Reporter ions were extracted within a small window ( $\pm 20$  ppm) around their anticipated  $m/z$  in the HCD spectrum. Protein abundances were computed from the sum of peptide abundances derived from TMT reporter ion intensities, subsequently log<sub>2</sub>-transformed and normalized through the column median method to account for equal loading across samples. Statistical analysis was executed using Perseus software (Version 1.6.15.0).

## 3. RESULTS

### 3.1. *Histologic assessments of ischemia-reperfusion injury*

#### 3.1.1. Effect of BX-001N treatment on myocardial tissue damage in rat IRI models

The effects of BX-001N treatment on myocardial infarct size was evaluated using the TTC assay, with the findings illustrated in Figure 4. Notably, administration of BX-001N at 40 mg/kg in the absence of IRI did not induce any myocardial tissue damage. Conversely, a marked increase in myocardial infarction was observed within the LAD territory in the IRI group compared to the sham group ( $p$ -value  $< 0.0001$ ). Importantly, BX-001N administration significantly attenuated myocardial damage in a dose-responsive manner. Within the IRI group, the average infarct size represented  $26.88 \pm 2.93\%$  of the myocardial tissue. Remarkably, this infarct dimension was significantly diminished in the bilirubin treatment group receiving 20 mg/kg ( $12.21 \pm 2.64\%$ ,  $p$ -value = 0.0001) and 40 mg/kg ( $8.81 \pm 1.47\%$ ,  $p$ -value  $< 0.0001$ ) of BX-001N.

#### 3.1.2. Effect of BX-001N treatment on myocardial apoptosis in rat IRI models

The extent of apoptosis within myocardial tissue was meticulously quantified utilizing the TUNEL assay (Figure 5). In the sham group, the apoptotic index (AI) in the non-infarcted myocardium was noted at  $10.72 \pm 0.79\%$ . The AI value increased significantly in the IRI group to  $20.52 \pm 1.65\%$ , indicating enhanced apoptosis. Notably, administration of BX-001N led to a significant decrease in the AI, with values of  $16.23 \pm 0.67\%$  at 20 mg/kg and  $14.68 \pm 1.00\%$  at 40 mg/kg, respectively. These findings support the potential therapeutic role of BX-001N in reducing myocardial apoptosis associated with IRI.

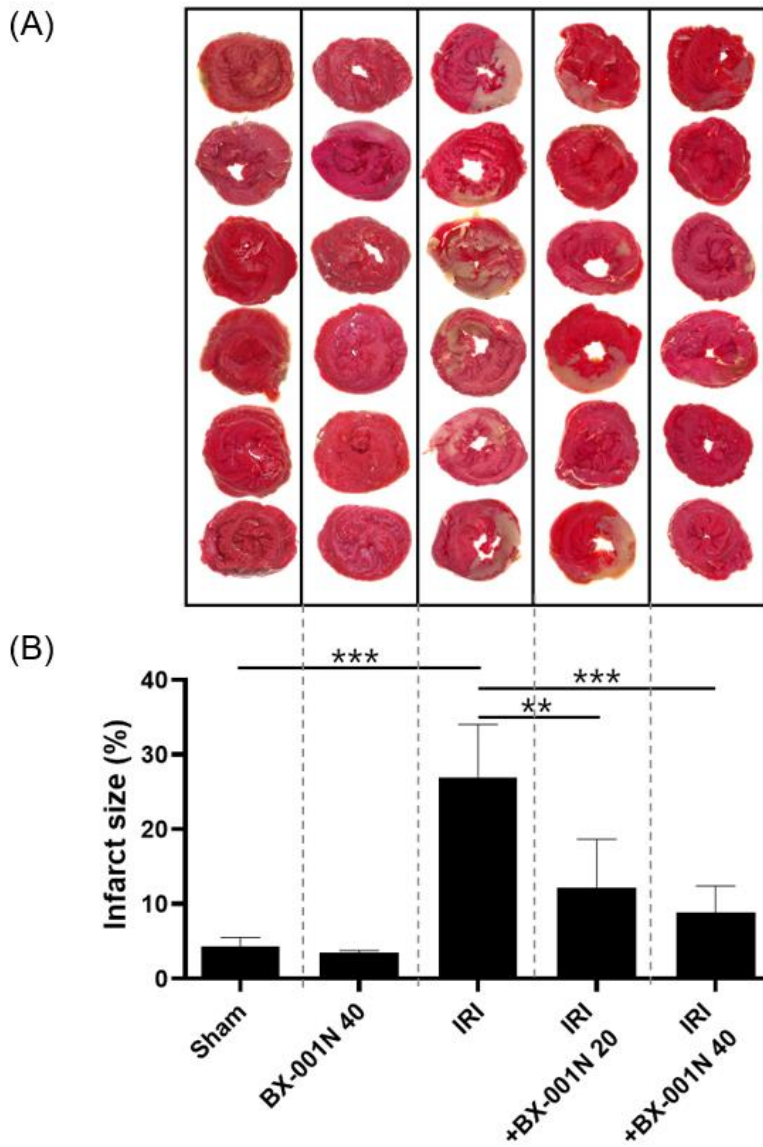


**Figure 4.** TTC staining analysis. (A) BX-001N treatment reduced infarct size in IRI rat models determined by the TTC assay. (B) Quantitative analysis of infarct sizes among different groups. Sham vs. IRI,  $p$ -value < 0.0001; IRI vs. IRI + BX-001N (20 mg/kg),  $p$ -value = 0.0001; IRI vs. IRI + BX-001N (40 mg/kg),  $p$ -value < 0.0001.

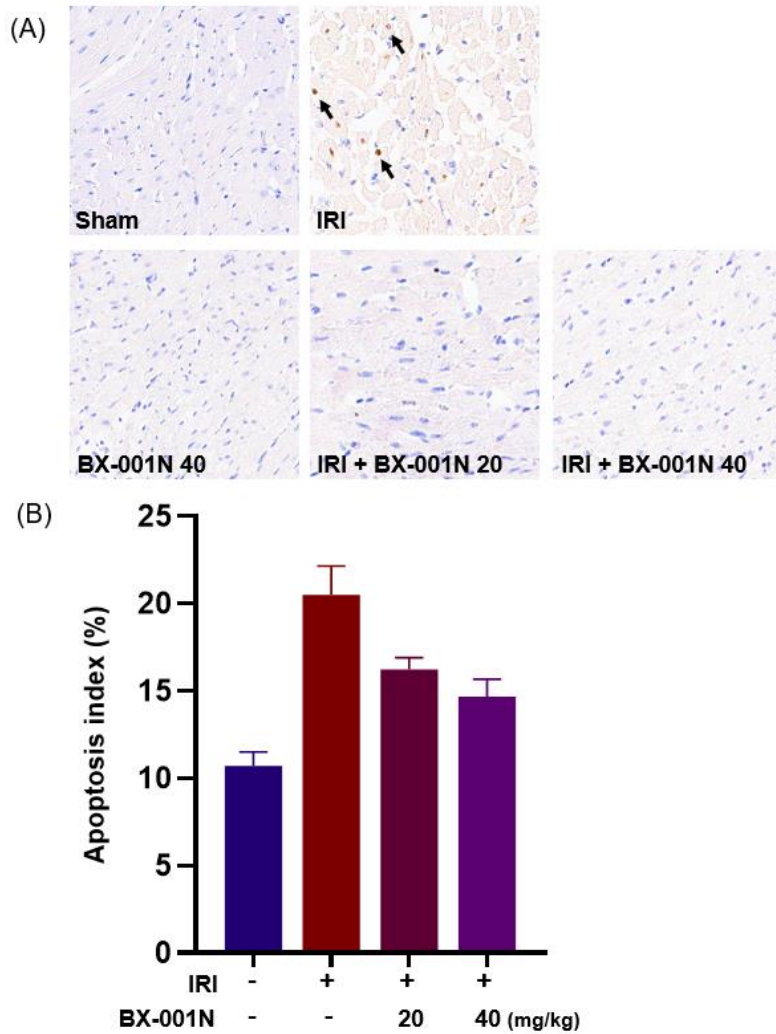


**Figure 5.** TUNEL staining. (A) TUNEL staining in myocardial tissue sections from each experimental group (magnification:  $\times 200$ ). (B) Quantification of apoptotic index (AI). The AI is quantified based on the number of TUNEL-positive cells (highlighted with black arrows in A), representing the proportion of apoptotic cells in the tissue sections. Sham vs. IRI,  $p$ -value  $< 0.0001$ ; IRI vs. IRI + BX-001N (20 mg/kg),  $p$ -value = 0.053; IRI vs. IRI + BX-001N (40 mg/kg),  $p$ -value = 0.0061.

### 3.2. *LC-MS/MS proteomics profiling*

To further investigate the impact of BX-001N treatment on LAD-ligated heart tissue, we performed proteomics analysis using LC-MS/MS on heart tissue from sacrificed rats (Figure 3). Analyzing 20 fraction RAW files, we identified a total of 8,560 protein groups with 76,681 distinct peptides, achieving a 1.0% FDR at both spectra and protein levels using ProteinInferencer, against the total 84,856 rat database including unreviewed entries. For protein quantification analysis, 3,616 protein groups with two or more unique peptides were selected, utilizing an in-house Python 3.9-coded program for spectra filtering with two global reference samples and the Bonferroni-Hochberg filtering method from a TMT-11-plex experiment (Figure 6). After the global normalization, sample similarity was assessed using Pearson's Correlation, with all comparisons showing an  $R^2$  value of 0.98 or higher. It is indicated that all tested samples have high comparability among them.

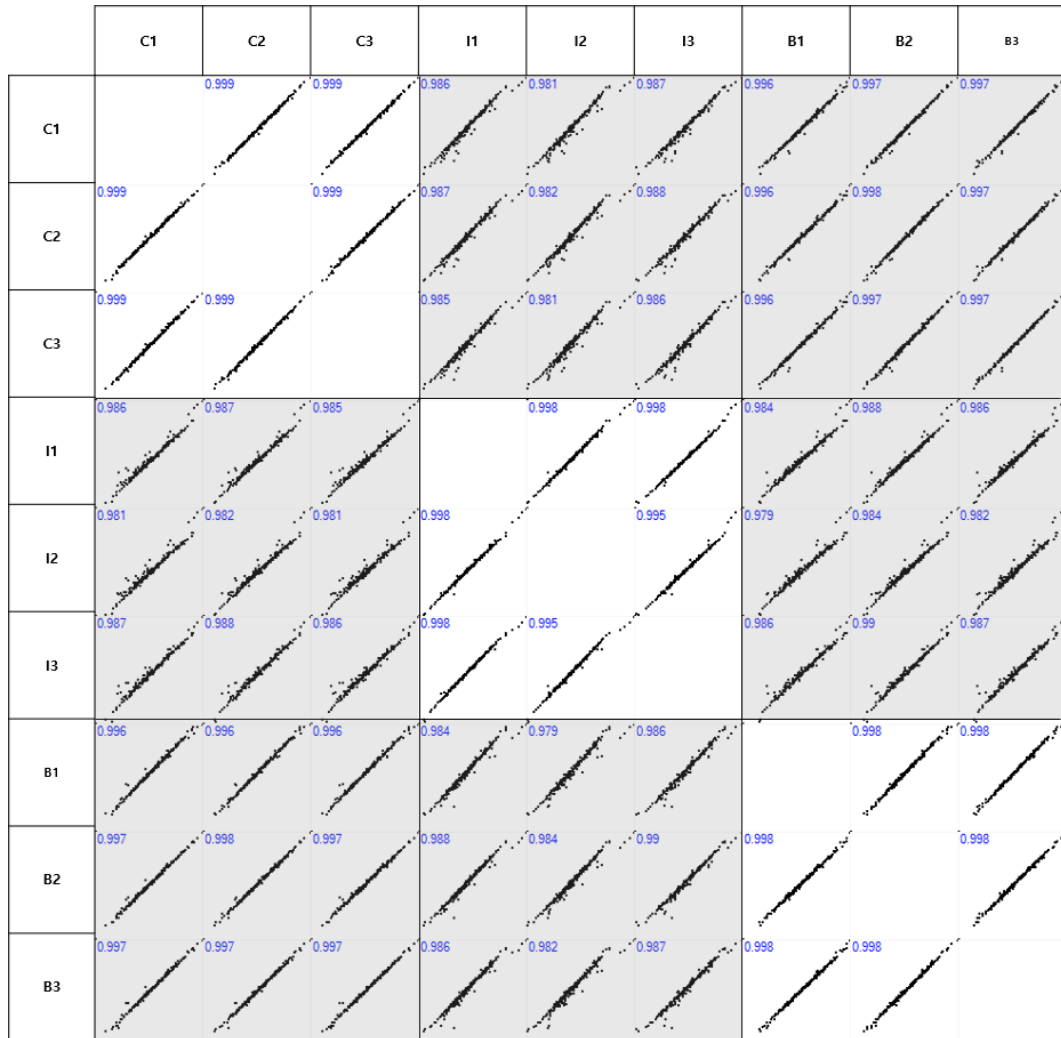


**Figure 6.** The Pearson correlation for each sample reveals values exceeding 0.98 within the same sample group.

Upon constructing a heatmap from the identified protein list using z-score normalization, distinct clustering patterns emerged, correlating with specific expression profiles. In our clustering analysis, we formed four distinct clusters with a threshold of 2.6478, grouping data points based on a similarity score exceeding this threshold. This revealed meaningful patterns and relationships, providing valuable insights into the dataset's structure. We identified two primary clusters of proteins, denoted as Cluster 0 (C0) and Cluster 1 (C1), each displaying unique expression patterns in response to different treatments (Figure 7). First, the C0 of 202 proteins shows down-regulated on IRI model and recovered on IRI + BX-001N treatment. The other hand, the C1 of 35 proteins shows up-regulated on IRI and recovered on IRI + BX-001N treatment. Finally, only five and two proteins were classified as the Cluster 2 (C2) and Cluster 3 (C3), respectively.

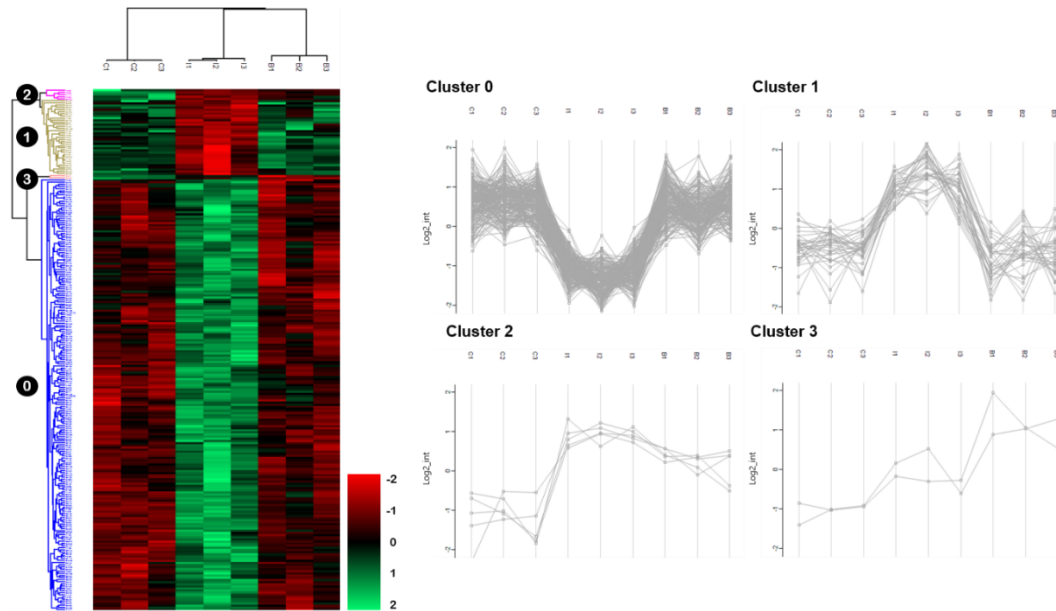


**Figure 7.** The heatmap of clustered samples revealed distinct patterns for each cluster. In this representation, the color red denotes an increase, while a decrease is represented by the color green. In Cluster 0, a noticeable reduction was observed in the IRI model, followed by an improvement upon the administration of IRI + BX-001N treatment. Conversely, in Cluster 1, an increase was evident during the IRI model, followed by a subsequent decrease upon BX-001N treatment.

### 3.3. *Bioinformatic analysis*

Particularly noteworthy is the behavior of proteins in C0 (Table 1). Upon conducting pathway analysis for proteins corresponding to C0, using Metascape, it was observed that Golgi-to-endoplasmic reticulum (ER) retrograde transport had the lowest  $-\log_{10}$  ( $p$ -value) of 10.029 (Figure 8A). Additionally, the Wnt signaling pathway and insulin signaling were identified with  $-\log_{10}$  ( $p$ -values) of 6.829 and 6.123, respectively. As discussed in the paper, these three pathways, with BX-001N treatment, show potential therapeutic effects. This suggests the possibility of therapeutic efficacy in BX-001N treatment, as indicated by these pathways.

Although C1 comprises 35 proteins, it holds significance as a group of proteins that are up-regulated in IRI but recover upon BX-001N treatment (Table 2). Pathway analysis revealed the identification of the nitric oxide transport pathway and the reactive oxygen species metabolic process, with  $-\log_{10}$  ( $p$ -value) of 7.359 and 5.715, respectively (Figure 8B). This suggests a correlation with BX-001N acting as a potent antioxidant. As observed in the paper, these findings underscore the meaningful impact of G1, displaying its role in the recovery of proteins affected by BX-001N treatment.

**Table 1.** Results of pathway analysis using the Metascape tool for cluster 0

Term	Description	Log <sub>10</sub> ( <i>p</i> -value)
R-RNO-8856688	Golgi-to-ER retrograde transport	-10.0292
R-RNO-9716542	Signaling by Rho GTPases, Miro GTPases and RHOBTB3	-9.88945
rno05132	Salmonella infection	-9.78415
R-RNO-199991	Membrane Trafficking	-9.2998
R-RNO-194315	Signaling by Rho GTPases	-9.29188
R-RNO-6811442	Intra-Golgi and retrograde Golgi-to-ER traffic	-9.12304
R-RNO-5653656	Vesicle-mediated transport	-8.91712
GO:0120035	Regulation of plasma membrane bounded cell projection organization	-7.96152
R-RNO-6807878	COPI-mediated anterograde transport	-7.66433
R-RNO-73887	Death Receptor Signaling	-7.29949
GO:0010975	regulation of neuron projection development	-7.04214
R-RNO-5357956	TNFR1-induced NF-kappa-B signaling pathway	-7.00573
R-RNO-199977	ER to Golgi Anterograde Transport	-7.00282
GO:0072659	Protein localization to plasma membrane	-6.9079
WP375	Wnt signaling pathway	-6.82917
GO:0016310	Phosphorylation	-6.72316
GO:0022604	Regulation of cell morphogenesis	-6.69262
CORUM:611	Exocyst complex	-6.65661
GO:0031346	Positive regulation of cell projection organization	-6.59416
GO:0051668	Localization within membrane	-6.56522
GO:1990778	Protein localization to cell periphery	-6.52182

R-RNO-6811434	COPI-dependent Golgi-to-ER retrograde traffic	-6.51283
R-RNO-446728	Cell junction organization	-6.38452
GO:0051640	Organelle localization	-6.36861
R-RNO-948021	Transport to the Golgi and subsequent modification	-6.2364
WP439	Insulin signaling	-6.12344
GO:0034330	Cell junction organization	-5.87974
R-RNO-6811436	COPI-independent Golgi-to-ER retrograde traffic	-5.8292
GO:0007030	Golgi organization	-5.81215
R-RNO-264876	Insulin processing	-5.69446
R-RNO-3371556	Cellular response to heat stress	-5.66558
GO:0051648	Vesicle localization	-5.58476
R-RNO-446203	Asparagine N-linked glycosylation	-5.55239
GO:0072657	protein localization to membrane	-5.54564
R-RNO-1500931	Cell-Cell communication	-5.53389
R-RNO-75893	TNF signaling	-5.51867
R-RNO-2262752	Cellular responses to stress	-5.45135
R-RNO-8953897	Cellular responses to stimuli	-5.41183
R-RNO-1266738	Developmental Biology	-5.39055
GO:0048193	Golgi vesicle transport	-5.3515
GO:0099175	Regulation of postsynapse organization	-5.33848
R-RNO-195258	RHO GTPase Effectors	-5.31573
GO:1905475	Regulation of protein localization to membrane	-5.27781
GO:0046578	Regulation of Ras protein signal transduction	-5.259
R-RNO-1632852	Macroautophagy	-5.24109

R-RNO-9612973	Autophagy	-5.24109
GO:0070966	Nuclear-transcribed mRNA catabolic process, no-go decay	-5.14551
GO:0050770	Regulation of axonogenesis	-5.03982
rno04510	Focal adhesion	-4.80779
R-RNO-1640170	Cell Cycle	-4.77091

---

**Table 2.** Results of pathway analysis using the Metascape tool for cluster 1

Term	Description	Log <sub>10</sub> ( <i>p</i> -value)
GO:0030185	Nitric oxide transport	-7.35859
R-RNO-1247673	Erythrocytes take up oxygen and release carbon dioxide	-7.20391
R-RNO-1237044	Erythrocytes take up carbon dioxide and release oxygen	-6.82741
R-RNO-1480926	O <sub>2</sub> /CO <sub>2</sub> exchange in erythrocytes	-6.82741
GO:0015670	Carbon dioxide transport	-6.7229
GO:0015671	Oxygen transport	-6.37323
GO:0015669	Gas transport	-5.87177
GO:0072593	Reactive oxygen species metabolic process	-5.71505
R-RNO-9711123	Cellular response to chemical stress	-5.43657
R-RNO-9707564	Cytoprotection by HMOX1	-5.39883
rno05143	African trypanosomiasis	-5.29517
GO:0019755	one-carbon compound transport	-4.9232
rno05144	Malaria	-4.87447
GO:0098869	Cellular oxidant detoxification	-4.23137
GO:1990748	Cellular detoxification	-3.96013
GO:0097237	Cellular response to toxic substance	-3.78683
GO:0098754	Detoxification	-3.75686
R-RNO-2262752	Cellular responses to stress	-3.50868
R-RNO-8953897	Cellular responses to stimuli	-3.4963
R-RNO-382551	Transport of small molecules	-3.01325
GO:0043434	Response to peptide hormone	-2.86764
GO:0009636	Response to toxic substance	-2.68807

GO:1901652	Response to peptide	-2.61819
GO:0070372	Regulation of ERK1 and ERK2 cascade	-2.54233
GO:0071375	Cellular response to peptide hormone stimulus	-2.49988
GO:1901653	Cellular response to peptide	-2.24854
GO:0032940	Secretion by cell	-2.23198
GO:0140352	Export from cell	-2.06694
GO:0036293	Response to decreased oxygen levels	-2.04363

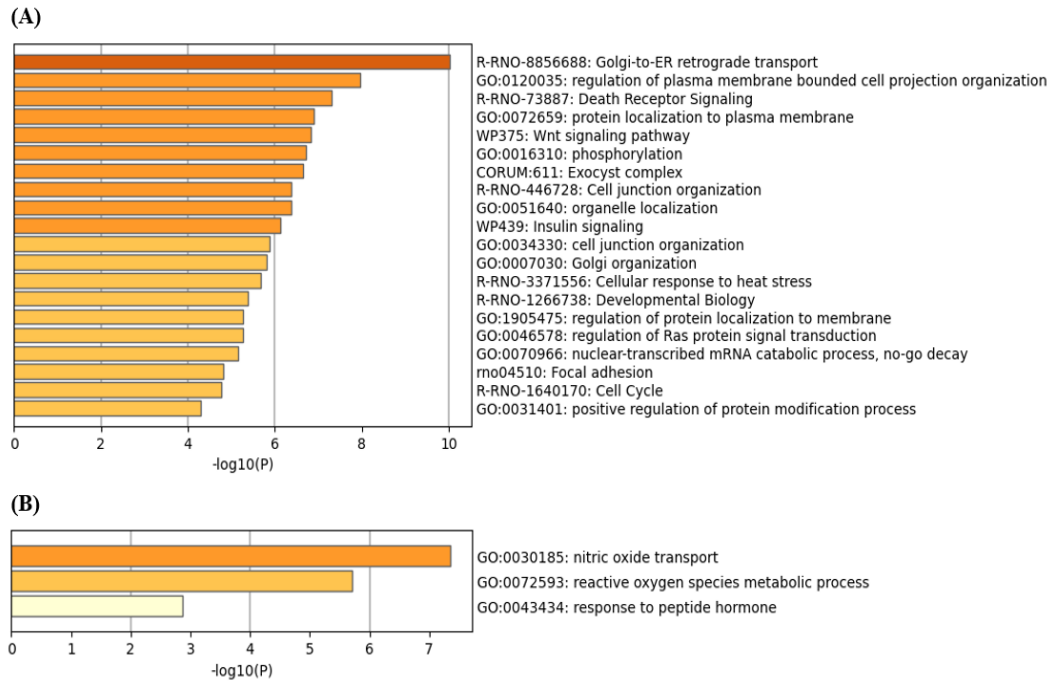
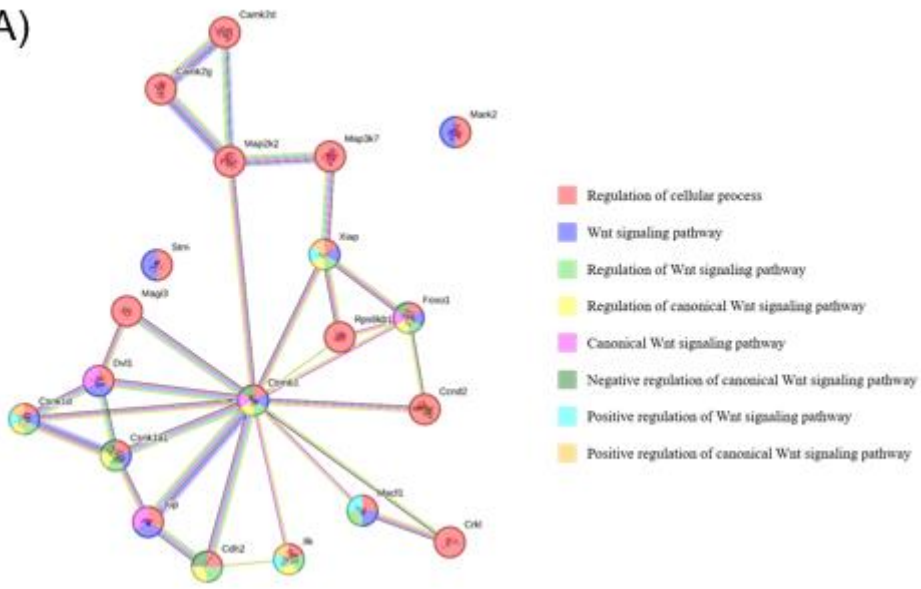


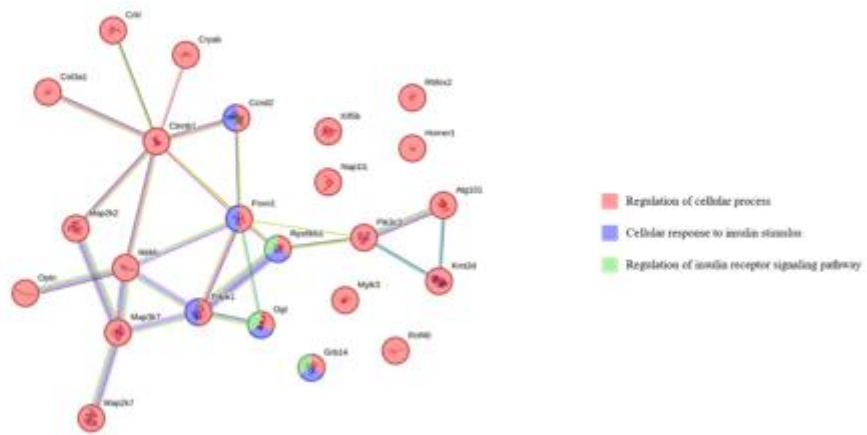
**Figure 8.** The outcomes of pathway analysis enriched via the Metascape web tool. This figure illustrates the results of pathway enrichment analyses for proteins identified in Cluster 0 and Cluster 1. (A) Pathway analysis for Cluster 0; down-regulated on IRI and recovered following IRI + BX-001N treatment. (B) Pathway analysis for Cluster 1; up-regulated on IRI and recovered following IRI + BX-001N treatment.

Further investigation into the proteins associated with the C0 was conducted using web-based tools such as STRING database (<https://string-db.org/>), and KEGG pathway database (<https://www.genome.jp/kegg/pathway.html>). Our analysis revealed the involvement in critical pathways including Wnt signaling, Golgi-to-ER retrograde transport, and insulin signaling from the STRING analysis result with interacting proteins of C0 (Figure 9). The outcomes of the STRING analysis underscored the intricate network of interconnections among various proteins related to Wnt signaling. We observed that the robust interaction landscape among proteins within C0 emphasizes their collective role in modulating the Wnt signaling pathway. From the result of KEGG pathway analysis, proteins associated with the main pathway of Wnt and Insulin signaling were also confirmed (Figure 10).

(A)



(B)



(C)

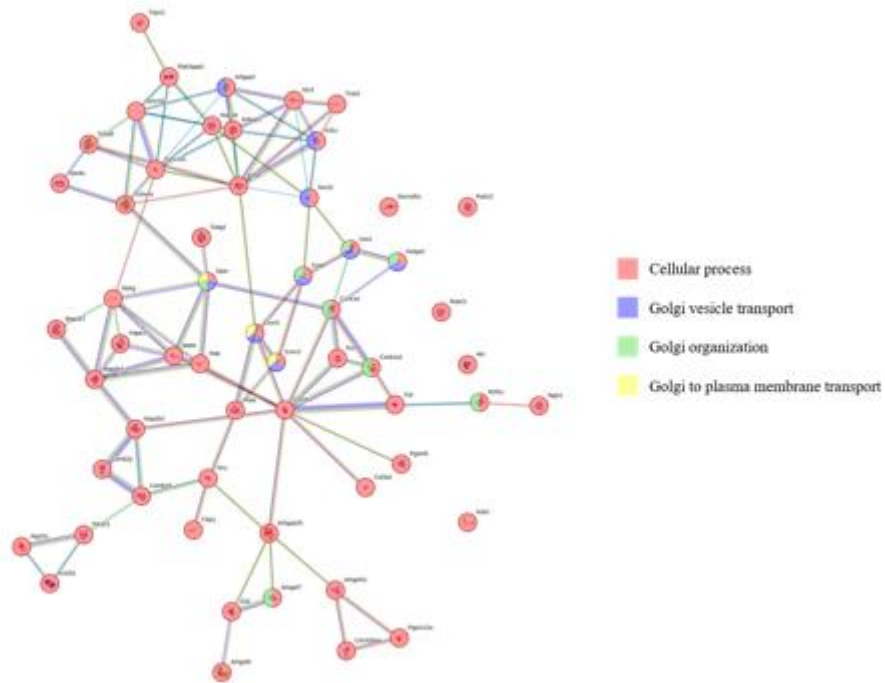


**Figure 9.** Pathway analysis results utilizing STRING database. (A) STRING analysis results for proteins associated with Wnt signaling, (B) STRING analysis results for proteins related to Insulin signaling, (C) STRING analysis results for proteins associated with Golgi-to-ER retrograde transport.

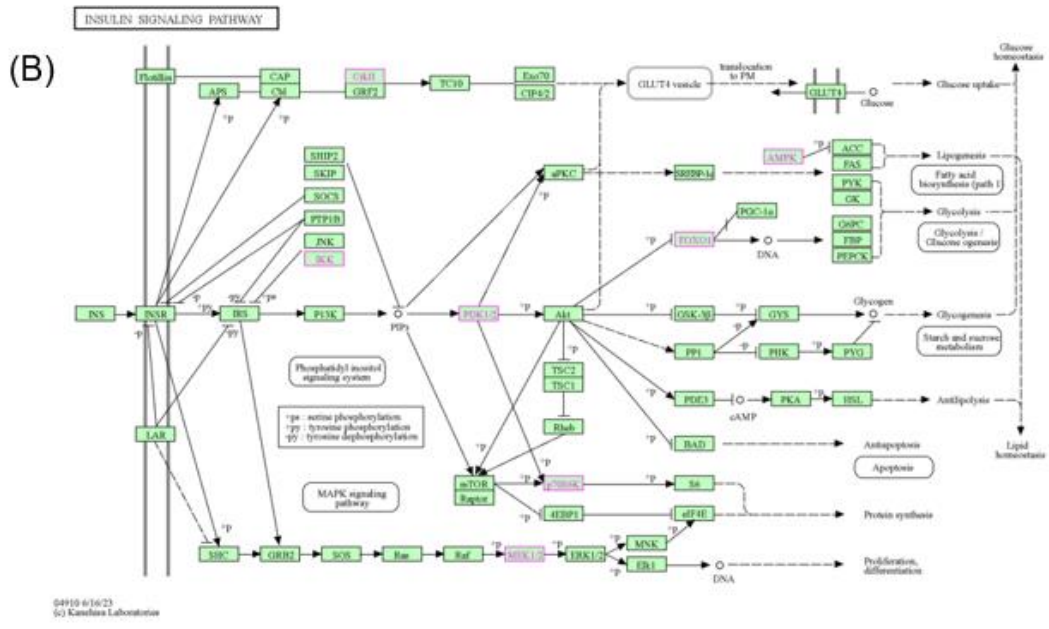
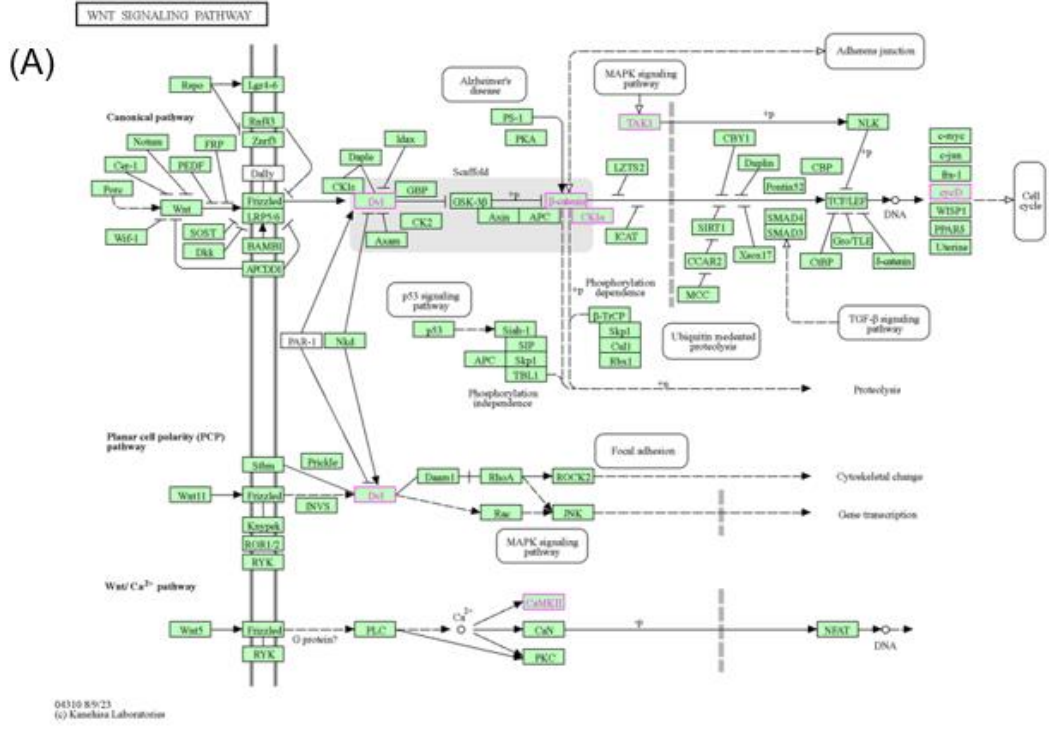


**Figure 10.** Pathway analysis results utilizing KEGG. (A) KEGG analysis results for proteins related to Wnt signaling, (B) KEGG analysis results for proteins associated with Insulin signaling.

## 4. DISCUSSION

In our study, we assessed the therapeutic efficacy of bilirubin nanoparticle (BX-001N) for mitigating myocardial tissue damage and apoptosis in rat IRI models. BX-001N treatment markedly reduced myocardial infarction and apoptosis in a dose-dependent manner, underscoring its cardioprotective properties against IRI. This suggests BX-001N's capability to mitigate myocardial injury and apoptosis effectively. Our proteomics analysis elucidated potential mechanisms, revealing upregulation in Wnt and insulin signaling pathways and increased Golgi markers following BX-001N treatment, which may underpin the cardioprotective effects observed.

Bilirubin, an endogenous metabolic end-product of heme catabolism, has historically been viewed as a harmful substance.<sup>9</sup> However, growing evidence reveals that bilirubin has potent antioxidant, anti-inflammatory, and immunomodulatory properties.<sup>10-12</sup> Accumulating clinical data suggest that bilirubin may confer protective benefits against various conditions, including IRI, cardiovascular and metabolic diseases, and may even reduce all-cause mortality.<sup>23-25</sup> Its beneficial roles extend into organ transplantation, positing bilirubin as a candidate with broad therapeutic implications.<sup>17,26</sup> Despite the promising therapeutic prospects of bilirubin, its clinical utility has been hampered by its insolubility and short half-life (< 5 minutes).<sup>19</sup> Recent technological advances in nanoparticle development have effectively addressed these challenges, overcoming the inherent hydrophobicity and rapid clearance of bilirubin.<sup>19-21</sup> Through encapsulating bilirubin within nanoparticles, its solubility is significantly enhanced and its systemic circulation time is extended, thereby augmenting its therapeutic utility.

Reperfusion of ischemic tissues triggers a series of detrimental effects, predominantly oxidative and inflammatory responses, which exacerbate cellular and organ damage.<sup>5-7</sup> Consequently, effective IRI management strategies necessitate interventions that can mitigate oxidative stress and attenuate inflammatory response. Given its recognized antioxidant and anti-inflammatory properties,

bilirubin emerges as a promising therapeutic agent for IRI management.<sup>18,21</sup> Experimental studies have confirmed protective role of bilirubin against IRI in crucial organs such as the heart, liver, kidneys, and intestines.<sup>15,16,27,28</sup> However, research on the use of bilirubin nanoparticles for IRI remains limited, particularly regarding the protective mechanisms of bilirubin nanoparticles against IRI.<sup>15,16</sup> In the present study, we employed a proteomics-driven approach to elucidate the protective mechanisms of bilirubin nanoparticles in rat models of IRI.

Over the past decade, the Biology/Disease-driven Human Proteome Project has made significant efforts for the Human Proteome Project HPP by focusing on understanding the roles of proteins in various biological states and diseases, facilitating the development of targeted therapies and advancing our knowledge in disease diagnostics and prognostics with human as well as model organism samples.<sup>29,30</sup> However, the proteomic approaches for IRI and an effective treatment have reported very rare.<sup>31,32</sup> Our proteomic analysis identified significant upregulation in the Wnt and insulin signaling pathways and increased Golgi markers, indicating their role in mediating bilirubin nanoparticle's protective effects.

The enhancement of the Wnt signaling pathway, as identified in our study, plays a critical role in both heart development and recovery following IRI.<sup>33-35</sup> The upregulation of this pathway may attenuate oxidative stress, partly by inhibiting oxidative enzymes like NADPH oxidase, which are activated during oxidative stress conditions.<sup>36</sup> Furthermore, the Wnt pathway significantly contributes to dampening inflammatory responses, particularly through the suppression of nuclear factor kappa B (NF- $\kappa$ B), a key transcription factor involved in regulating inflammation and cell death.<sup>37,38</sup> The dual function of the Wnt pathway in mitigating oxidative stress and inflammation offers a plausible explanation for the protective effects of bilirubin in myocardial IRI.

As the Wnt signaling pathway encompasses various signaling branches, previous studies have demonstrated the multifaced roles of Wnt signaling in myocardial IRI (Table 3).<sup>39</sup> When activated, Wnt/ $\beta$ -catenin promotes inflammation, extracellular matrix remodeling, angiogenesis, and fibrosis.<sup>40</sup> Conversely, its inhibition during ischemia can lead to increased oxidative stress.<sup>41</sup>

Activation of the Wnt/planar cell polarity (PCP) pathway during ischemia promotes inflammation and cell hypertrophy, while during reperfusion, inhibition of Wnt/ $\beta$ -catenin signaling is associated with promoting apoptosis, inflammation, and cell hypertrophy.<sup>42,43</sup> Activation of Wnt/PCP and Wnt/ $\text{Ca}^{2+}$  pathways during reperfusion further promotes apoptosis, inflammation, and angiogenesis.<sup>44,45</sup>

Currently, several therapeutic strategies targeting the Wnt signaling pathway are being explored for the treatment of IRI.<sup>39,43</sup> These strategies aim to modulate different branches of the Wnt signaling pathway to confer cardioprotection (Table 4). Our findings suggest that bilirubin nanoparticles may offer an additional therapeutic approach by modulating the Wnt signaling pathway, warranting further investigation in future studies.

**Table 3.** Effect of Wnt signaling pathways during myocardial ischemia-reperfusion injury

Phase	Wnt signaling	Activity	Effect
Ischemia	Wnt/ $\beta$ -catenin	Activated	Promoting inflammation, extracellular matrix remodeling, angiogenesis, fibrosis
	Wnt/ $\beta$ -catenin	Inhibited	Promoting oxidative stress
	Wnt/PCP	Activated	Promoting inflammation, cell hypertrophy
Reperfusion	Wnt/ $\beta$ -catenin	Inhibited	Promoting apoptosis inflammation, cell hypertrophy
	Wnt/PCP	Activated	Promoting apoptosis, inflammation, angiogenesis
	Wnt/ $\text{Ca}^{2+}$	Activated	Promoting apoptosis

Abbreviation: PCP, planar cell polarity.

**Table 4.** Therapeutic strategies targeting Wnt signaling for the treatment of ischemia-reperfusion injury

Target pathways	Strategies	Effects
Active Wnt/ $\beta$ -catenin pathway	Exosomes isolated from adipose-derived Mesenchymal stem cells	Up-regulate Wnt3a; Inhibiting apoptosis
	Down-regulated miR-148b	Up-regulate Wnt1; Inhibiting apoptosis and oxidative damage
	Up-regulation of LncRNA AZIN1-AS1	Inhibiting apoptosis
	A polypeptide of tuna stem protein	Inhibiting apoptosis
	GSK3 $\beta$ inhibitor	Inhibiting apoptosis and cell hypertrophy
Inhibit Wnt/ $\beta$ -catenin pathway	Dexamethasone	Inhibit Wnt3a and Wnt5a; Inhibiting apoptosis
	Huoxin pill	Inhibit NF- $\kappa$ B; Inhibiting inflammation
Inhibit Wnt non-canonical pathways	Up-regulation of Sfrp5	Inhibit Wnt5a/JNK and Wnt/PCP; Inhibiting apoptosis and inflammation

Abbreviation: GSK, glucogen synthase kinase; JNK, c-Jun N-terminal kinase; NF- $\kappa$ B, nuclear factor- $\kappa$ B; PCP, planar cell polarity; Sfrp5, secreted frizzled-related protein 5.

Our data show an upregulation of insulin signaling pathways, which might confer protection against myocardial IRI. This increase in insulin signaling could potentially mitigate oxidative stress, possibly through a reduction in reactive oxygen species production.<sup>46</sup> Additionally, insulin signaling is also associated with the inhibition of NF- $\kappa$ B activation, thereby contributing to its anti-inflammatory effects.<sup>47</sup> Consequently, the enhanced insulin signaling observed following bilirubin nanoparticle treatment appears to provide myocardial protection through both its anti-oxidative and anti-inflammatory actions.

Moreover, the increased expression of Golgi markers in our study points to bilirubin's potential influence on myocardial IRI by modulating ER stress and enhancing Golgi function. The ER is crucial for protein synthesis, modification, and processing, playing a key role in maintaining cellular balance.<sup>48</sup> However, ischemic-reperfusion injury disrupts ER function, leading to the accumulation or misfolding of proteins.<sup>49</sup> While the exact molecular mechanisms of how bilirubin nanoparticle affects Golgi dynamics and ER stress modulation are not fully understood, our initial findings point to a complex interaction between bilirubin, ER stress, and Golgi function in the intricate scenario of myocardial IRI.

While bilirubin's antioxidant and anti-inflammatory properties are well-documented, our study enhances this understanding by utilizing bilirubin nanoparticle to improve bilirubin's solubility and bioavailability, thereby overcoming its traditionally rapid clearance and poor solubility. Our findings indicate that the modulation of specific signaling pathways, notably Wnt and insulin, may represent the mechanisms through which bilirubin nanoparticles exert their protective effects against oxidative stress and inflammation, pivotal factors in the pathogenesis of IRI. These insights provide a foundational understanding of the potential mechanisms underpinning the cardioprotective role of bilirubin nanoparticles in myocardial IRI, highlighting the necessity for further detailed investigations. Future research should focus on elucidating the exact molecular interactions and pathways by which bilirubin nanoparticles confer cardioprotection. Additionally, studies employing

human models of IRI are essential to ascertain the translational value of these findings and to assess the clinical feasibility of bilirubin nanoparticles as a therapeutic strategy for IRI.

## 5. CONCLUSION

In conclusion, our study uncovers a multifaceted network of cellular responses to bilirubin nanoparticle treatment in myocardial IRI, including the upregulation of Wnt and insulin signaling pathways and the enhancement of Golgi functions. This presents promising avenues for future research in cardiac protection strategies, potentially offering novel therapeutic approaches for myocardial ischemia-reperfusion injury.

## References

1. Eltzschig HK, Eckle T. Ischemia and reperfusion--from mechanism to translation. *Nat Med* 2011;17:1391-1401.
2. Yellon DM, Hausenloy DJ. Myocardial reperfusion injury. *N Engl J Med* 2007; 357:1121-1135.
3. Fernández AR, Sánchez-Tarjuelo R, Cravedi P, Ochando J, López-Hoyos M. Review: Ischemia Reperfusion Injury-A Translational Perspective in Organ Transplantation. *Int J Mol Sci* 2020;21:8549.
4. Lesnefsky EJ, Tandler B, Ye J, Slabe TJ, Turkaly J, Hoppel CL. Myocardial ischemia decreases oxidative phosphorylation through cytochrome oxidase in subsarcolemmal mitochondria. *Am J Physiol* 1997;273:H1544-1554.
5. Wu MY, Yiang GT, Liao WT, et al. Current Mechanistic Concepts in Ischemia and Reperfusion Injury. *Cell Physiol Biochem* 2018;46:1650-1667.
6. Frank A, Bonney M, Bonney S, Weitzel L, Koeppen M, Eckle T. Myocardial ischemia reperfusion injury: from basic science to clinical bedside. *Semin Cardiothorac Vasc Anesth* 2012;16:123-132.
7. Kurian GA, Rajagopal R, Vedantham S, Rajesh M. The Role of Oxidative Stress in Myocardial Ischemia and Reperfusion Injury and Remodeling: Revisited. *Oxid Med Cell Longev* 2016;2016:1656450.
8. Heusch G. Myocardial ischaemia-reperfusion injury and cardioprotection in perspective. *Nat Rev Cardiol* 2020;17:773-789.
9. Rodrigues CM, Solá S, Brites D. Bilirubin induces apoptosis via the mitochondrial pathway in developing rat brain neurons. *Hepatology* 2002;35:1186-1195.
10. Boon AC, Bulmer AC, Coombes JS, Fassett RG. Circulating bilirubin and defense against kidney disease and cardiovascular mortality: mechanisms contributing to protection in

- clinical investigations. *Am J Physiol Renal Physiol* 2014;307:F123-136.
11. Vitek L, Hinds TD, Jr., Stec DE, Tiribelli C. The physiology of bilirubin: health and disease equilibrium. *Trends Mol Med* 2023;29:315-328.
  12. Novák P, Jackson AO, Zhao GJ, Yin K. Bilirubin in metabolic syndrome and associated inflammatory diseases: New perspectives. *Life Sci* 2020;257:118032.
  13. Horsfall LJ, Nazareth I, Petersen I. Cardiovascular events as a function of serum bilirubin levels in a large, statin-treated cohort. *Circulation* 2012;126:2556-2564.
  14. Djoussé L, Levy D, Cupples LA, Evans JC, D'Agostino RB, Ellison RC. Total serum bilirubin and risk of cardiovascular disease in the Framingham offspring study. *Am J Cardiol* 2001;87:1196-1200.
  15. Kim JY, Lee DY, Kang S, et al. Bilirubin nanoparticle preconditioning protects against hepatic ischemia-reperfusion injury. *Biomaterials* 2017;133:1-10.
  16. Ai W, Bae S, Ke Q, et al. Bilirubin Nanoparticles Protect Against Cardiac Ischemia/Reperfusion Injury in Mice. *J Am Heart Assoc* 2021;10:e021212;2021.
  17. Lee J, Kim EJ, Lee JG, et al. Clinical impact of serum bilirubin levels on kidney transplant outcomes. *Sci Rep* 2021;11:6889.
  18. Adin CA. Bilirubin as a Therapeutic Molecule: Challenges and Opportunities. *Antioxidants (Basel)* 2021;10:1536.
  19. Lee Y, Kim H, Kang S, Lee J, Park J, Jon S. Bilirubin Nanoparticles as a Nanomedicine for Anti-inflammation Therapy. *Angew Chem Int Ed Engl* 2016;55:7460-7463.
  20. Park SJ, Lim JH, Lee J, et al. Investigation of pharmacokinetic properties of a PEGylated bilirubin nanoparticle in male Sprague-Dawley rats using liquid chromatography-quadrupole time-of-flight mass spectrometry. *Xenobiotica* 2023; 2284859:1-36.
  21. Yao Q, Chen R, Ganapathy V, Kou L. Therapeutic application and construction of bilirubin incorporated nanoparticles. *J Control Release* 2020;328:407-424.
  22. Cho SY, Hwang H, Kim YH, et al. Refining Classification of Cholangiocarcinoma

- Subtypes via Proteogenomic Integration Reveals New Therapeutic Prospects. *Gastroenterology* 2023;164:1293-1309.
23. Temme EH, Zhang J, Schouten EG, Kesteloot H. Serum bilirubin and 10-year mortality risk in a Belgian population. *Cancer Causes Control* 2001;12:887-894.
  24. Lin JP, O'Donnell CJ, Schwaiger JP, et al. Association between the UGT1A1\*28 allele, bilirubin levels, and coronary heart disease in the Framingham Heart Study. *Circulation* 2006;114:1476-1481.
  25. Liu M, Li Y, Li J, Lv X, He Y. Elevated serum total bilirubin levels are negatively associated with major diabetic complications among Chinese senile diabetic patients. *J Diabetes Complications* 2017;31:213-217.
  26. Sundararaghavan VL, Binepal S, Stec DE, Sindhwani P, Hinds TD, Jr. Bilirubin, a new therapeutic for kidney transplant? *Transplant Rev (Orlando)* 2018;32:234-240.
  27. Hammerman C, Goldschmidt D, Caplan MS, et al. Protective effect of bilirubin in ischemia-reperfusion injury in the rat intestine. *J Pediatr Gastroenterol Nutr* 2002;35:344-349.
  28. Adin CA, Croker BP, Agarwal A. Protective effects of exogenous bilirubin on ischemia-reperfusion injury in the isolated, perfused rat kidney. *Am J Physiol Renal Physiol* 2005;288:F778-784.
  29. Aebersold R, Bader GD, Edwards AM, et al. The biology/disease-driven human proteome project (B/D-HPP): enabling protein research for the life sciences community. *J Proteome Res* 2013;12:23-27.
  30. Tholey A, Taylor NL, Heazlewood JL, Bendixen E. We Are Not Alone: The iMOP Initiative and Its Roles in a Biology- and Disease-Driven Human Proteome Project. *J Proteome Res* 2017;16:4273-4280.
  31. Zhu XM, Tan Y, Shi YH, et al. TMT-based quantitative proteomics analysis of the effects of Jiawei Danshen decoction myocardial ischemia-reperfusion injury. *Proteome Sci*

- 2022;20:17.
32. Yao L, He F, Zhao Q, et al. Spatial Multiplexed Protein Profiling of Cardiac Ischemia-Reperfusion Injury. *Circ Res* 2023;133:86-103.
  33. Gessert S, Kühl M. The multiple phases and faces of wnt signaling during cardiac differentiation and development. *Circ Res* 2010;107:186-199.
  34. Oerlemans MI, Goumans MJ, van Middelaar B, Clevers H, Doevendans PA, Sluijter JP. Active Wnt signaling in response to cardiac injury. *Basic Res Cardiol* 2010;105:631-641.
  35. Paik DT, Rai M, Ryzhov S, et al. Wnt10b Gain-of-Function Improves Cardiac Repair by Arteriole Formation and Attenuation of Fibrosis. *Circ Res* 2015;117:804-816.
  36. Tang Y, Shen J, Zhang F, Yang FY, Liu M. Human serum albumin attenuates global cerebral ischemia/reperfusion-induced brain injury in a Wnt/ $\beta$ -Catenin/ROS signaling-dependent manner in rats. *Biomed Pharmacother* 2019;115:108871.
  37. Ma B, Hottiger MO. Crosstalk between Wnt/ $\beta$ -Catenin and NF- $\kappa$ B Signaling Pathway during Inflammation. *Front Immunol* 2016;7:378.
  38. Chen S, Guttridge DC, You Z, et al. Wnt-1 signaling inhibits apoptosis by activating beta-catenin/T cell factor-mediated transcription. *J Cell Biol* 2001;152:87-96.
  39. Zhnag M, Liu Q, Meng H, et al. Ischemia-reperfusion injury: molecular mechanisms and therapeutic targets. *Signal Transduct Target Ther* 2024;9:12.
  40. Palevski D, Levin-Kotler LP, Kain D et al. Loss of macrophage Wnt secretion improves remodeling and function after myocardial infarction in mice. *J Am Heart Assoc* 2017;6:e004387.
  41. Shen J, Li Y, Jiao Y, et al. Wnt 3a protects myocardial injury in elderly acute myocardial infarction by inhibiting serum cystatin C/ROS-induced mitochondrial damage. *Front Physiol* 2022: 13:950960.
  42. Matsushima K, Suyama T, Takenaka C, et al. Secreted frizzled related protein 4 reduces fibrosis scar size and ameliorates cardiac function after ischemic injury. *Tissue Eng Part A*

- 2010;16:3329–41.
43. Yang M, Kong DY, Chen JC, et al. Inhibition of miR-148b ameliorates myocardial ischemia/reperfusion injury via regulation of Wnt/beta-catenin signaling pathway. *J Cell Physiol* 2019;234:17757-17766.
  44. Nakamura K, Sano S, Fuster JJ, et al. Secreted Frizzled-related Protein 5 Diminishes Cardiac Inflammation and Protects the Heart from Ischemia/Reperfusion Injury. *J Biol Chem* 2016;291:2566-2575
  45. Zhou SS, He F, Chen AH, et al. Suppression of rat Frizzled-2 attenuates hypoxia/reoxygenation-induced  $Ca^{2+}$  accumulation in rat H9C2 cells. *Exp Cell Res* 2012;318:1480-1491.
  46. Lennicke C, Cochemé HM. Redox regulation of the insulin signalling pathway. *Redox Biol* 2021;42:101964.
  47. Baker RG, Hayden MS, Ghosh S. NF- $\kappa$ B, inflammation, and metabolic disease. *Cell Metab* 2011;13:11-22.
  48. Hetz C, Papa FR. The Unfolded Protein Response and Cell Fate Control. *Mol Cell* 2018;69:169-181.
  49. Minamino T, Komuro I, Kitakaze M. Endoplasmic reticulum stress as a therapeutic target in cardiovascular disease. *Circ Res* 2010;107:1071-1082.

## Abstract in Korean

### 빌리루빈 나노파티클의 심장 허혈-재관류 손상 보호 효과

심근경색은 관상동맥 혈류가 차단되는 허혈 시 발생하는데, 이 때 심장의 비가역적 손상을 막기 위해서는 최대한 빨리 혈류가 통할 수 있도록 재관류 치료가 필요하다. 그러나 역설적으로 재관류 치료를 시행하면 심장 조직에 추가적인 허혈-재관류 손상이 발생한다. 허혈-재관류 손상은 허혈이 발생한 조직에 혈류가 복원될 때 산화 스트레스와 염증 반응을 통해 조직 손상이 발생하는 현상으로 현재까지 효과적인 치료법이 없다. 빌리루빈은 헴 (Heme) 대사 과정에서 발생하는 산물로 체내에서 가장 강력한 항산화 및 항염증 효과를 갖는 물질이다. 이러한 항산화 및 항염증 작용으로 미루어 심장의 허혈-재관류 손상에 대해 빌리루빈의 치료 효과를 기대해 볼 수 있다. 본 연구는 백서 심근 허혈-재관류 손상 모델에서 빌리루빈 나노파티클 치료 효과를 조사하였다. 또한 액체 크로마토그래피-질량 분석법을 이용하여 단백질학 분석을 수행하여 빌리루빈 나노파티클 치료의 허혈-재관류 손상 방어 메커니즘을 규명하고자 하였다. 빌리루빈 나노파티클 치료는 심근 허혈-재관류 손상 모델에서 용량 의존적으로 심근 경색 면적 및 세포사멸을 유의하게 감소시켰다. 단백질 프로파일링 결과, 총 3,616개의 단백질 그룹과 76,681개의 펩타이드를 확인하였다. 이들 단백질에 대해 허혈-재관류 손상 및 빌리루빈 나노파티클 치료 시 나타나는 패턴에 따라 클러스터링 분석을 수행하였다. 그 결과, 심근 허혈-재관류 손상 모델에서 202개의 단백질이 감소하였으며, 빌리루빈 나노파티클 치료 후 회복되었다. 반면에, 35개의 단백질은 허혈-재관류 손상 시 증가하였으나, 빌리루빈

나노파티클 치료 후에 감소했다. 경로 분석을 통해 이들 단백질 변화는 Wnt 신호 및 인슐린 신호 경로의 강화와 골지체 마커의 증가와 연관된 것으로 나타났다. 이는 빌리루빈 나노파티클이 심근 허혈-재관류 손상에 대항하여 보호 효과를 발휘하는 메커니즘을 제시하였다. 향후 사람을 대상으로 하는 임상 모델에서의 추가 연구를 통해 빌리루빈 나노파티클의 임상적 적용 가능성을 탐색할 필요가 있다.

---

핵심되는 말 : 허혈-재관류 손상, 심장, 빌리루빈 나노파티클, 단백질체학